A modell for fragmentation of hard metallic targets due to shaped charge jet perforation

GUNNAR WIJK

FOI is an assignment-based authority under the Ministry of Defence. The core activities are research, method and technology development, as well as studies for the use of defence and security. The organization employs around 1350 people of whom around 950 are researchers. This makes FOI the largest research institute in Sweden. FOI provides its customers with leading expertise in a large number of fields such as security-policy studies and analyses in defence and security, assessment of different types of threats, systems for control and management of crises, protection against and management of hazardous substances, IT-security an the potential of new sensors.

FOI
Defence Research Agency
Weapons and Protection
SE-147 25 Tumba

Phone: +46 8 555 030 00
Fax: +46 8 555 031 00

www.foi.se

FOI-R-- 1751 --SE
ISSN 1650-1942

Weapons and Protection
Scientific report

November 2005

A modell for fragmentation of hard metallic targets due to shaped charge jet perforation

FOI-R--1751--SE
ISSN 1650-1942

Weapons and Protection
Scientific report

November 2005

Issuing organization	Report number, ISRN	Report type
FOI – Swedish Defence Research Agency Weapons and Protection SE-147 25 Tumba	FOI-R--1751--SE	Scientific report
	Research area code 5. Strike and protection	
	Month year November 2005	**Project no.** E2007
	Sub area code 51 Weapons and Protection	
	Sub area code 2	

Author/s (editor/s)	Project manager
Gunnar Wijk	**Approved by**
	Sponsoring agency
	Scientifically and technically responsible

Report title

A modell for fragmentation of hard metallic targets due to shaped charge jet perforation

Abstract

New models for rigid and eroding projectile penetration and perforation including production of target fragments have been suggested. Furthermore, the model for eroding projectile penetration has been extended to shaped charge jet penetration. The present report extends the model for projectile production of target fragments to describe such production with shaped charge jets. Comparison with experimental results shows reasonably good agreement. The intended application of these models is in computer programs for assessment of the effects on and the vulnerability of complex targets such as tanks, fighter aircraft and naval ships.

Keywords

Fragments, shaped charge, perforation, model

Further bibliographic information	Language English
ISSN 1650-1942	**Pages** 18 p.
	Price acc. to pricelist

Utgivare FOI - Totalförsvarets forskningsinstitut Vapen och skydd 147 25 Tumba	**Rapportnummer, ISRN** FOI-R--1751--SE	**Klassificering** Vetenskaplig rapport
	Forskningsområde 5. Bekämpning och skydd	
	Månad, år November 2005	**Projektnummer** E2007
	Delområde 51 VVS med styrda vapen	
	Delområde 2	

Författare/redaktör Gunnar Wijk	**Projektledare**
	Godkänd av
	Uppdragsgivare/kundbeteckning
	Tekniskt och/eller vetenskapligt ansvarig

Rapportens titel

Modell för splitterproduktion vid RSV-genomträngning av hårda metalliska mål

Sammanfattning

Nya modeller har föreslagits för stela och eroderande projektilers inträngning i och genomträngning av hårda metalliska mål, varvid det senare inkluderar fragmentering av målmaterialet. Vidare har modellen för eroderande projetiler utvidgats till att omfatta RSV-inträngning. Föreliggande rapport utvidgar modellen för projektilers fragmentering av målet till att också gälla för RSV-strålar. Jämförelse med experimentell resultat visar hygglig överensstämmelse. Den avsedda tillämningen av dessa modeller är för vrdering av verkan och sårbarhet för komplexa mål som stridvagnar, stridsflygplan och örlogsfartyg.

Nyckelord

Splitter, RSV, genomträngning, modell

Övriga bibliografiska uppgifter	**Språk** Engelska
ISSN 1650-1942	**Antal sidor:** 18 s.
Distribution enligt missiv	**Pris: Enligt prislista**

Nomenclature

B	non-dimensional parameter in mass distribution of target fragments
C	SC (Shaped Charge) caliber, m
D_T	hole diameter in target material, m
d_P	projectile or SC jet fragment diameter, m
E_T	elastic modulus of target material, Pa
F	action-and–reaction force during acceleration of target fragments, N
h	target thickness, m
h^*	thickness of plug that becomes target fragments, m
L	partial length of SC jet, m
L_P	accumulated length of fragmented SC jet, m
L_P^*	accumulated length of SC jet that produces target fragments, m
l_P	length of a SC jet fragment, m
M	accumulated mass of target fragments, kg
m_P^*	mass of SC jet fragments that produce target fragments, kg
m_T	total mass of fragments from rear target surface, kg
m_i	mass of i^{th} target fragment from rear target surface, kg
n	number of target fragment
P	SC jet penetration depth, m
S	stand-off distance, m
S_{opt}	optimum stand-off distance, m
t	thickness of SC insert, m
u_{exit}	exit velocities of foremost target fragments, m/s
v	SC jet fragment velocity, m/s
v_{front}	SC jet front velocity, m/s
$v_{\lim}$	smallest SC jet fragment velocity that contributes significantly to penetration depth, m/s
v_{exit}	exit velocity of foremost-and-outermost target fragment, m/s
W	energy, J
Y_T	uniaxial yield strength for target material, Pa
α	fraction of SC insert that becomes SC jet
β_T	target deformation parameter (non-dimensional penetration resistance)
λ	non-dimensional parameter in mass distribution of target fragments
ρ_P	density of SC jet material, kg/m^3
ρ_T	target density, kg/m^3
τ	time required for acceleration of target fragments, s
Ψ	maximum angle between SC jet direction and target fragment direction
Ψ_T	non-dimensional hole size parameter
v_T	characteristic target velocity parameter, m/s
θ	half apex angle of SC conical insert
ϑ	angle between SC jet direction and target fragment direction

Introduction

A new model for projectile penetration and perforation of hard steel and metallic target plates has been suggested in previous papers [1 - 5]. Projectiles are labelled as either rigid or eroding depending on the combination of relevant projectile and target parameters. When a projectile is sufficiently close to the rear surface of the target, then an eroding projectile may be assumed to become rigid or continue to be eroded. The remaining perforation phase involves production of fragments from the target. The papers [1 - 3] describe the different situations that may occur and yield the corresponding total masses of fragments. The paper [4] suggests a model for the distribution of fragment masses and the corresponding velocities and directions of motion for all fragments. The paper [5] extends the model for eroding projectile penetration to describe penetration with a shaped charge (SC) jet, which is considered to be a stream of small eroding projectiles with negligible strength and decreasing impact velocity. The present paper suggests how the

models in the papers [4, 5] should be combined to account for production of target fragments from SC jet perforation.

Model for the hole diameter

In [3 - 5] it is assumed that the diameter D_T of a hole, which is produced by an eroding projectile with diameter d_P and instantaneous velocity v, is given by

$$D_T = d_P \frac{v}{v_T} \tag{1}$$

with

$$v_T = \psi_T \sqrt{\frac{\beta_T Y_T}{\rho_T}} . \tag{2}$$

Here Y_T, ρ_T and β_T are the target material yield strength, density and penetration resistance coefficient, respectively. With hard target materials a representative value for the latter is β_T=5. v_T is a characteristic velocity parameter and ψ_T is a non-dimensional coefficient, which experimentally is found to be in the interval $1.1<\psi_T<1.5$ for aluminum, copper and steel and also for alloys of tungsten with small fractions of cobalt and similar binding materials. Possibly ψ_T may be independent of the projectile material, but it is more likely that it decreases marginally with the ratio ρ_T/ρ_P between the target and projectile densities. Presently there is not sufficient experimental information to suggest such dependence quantitatively, mainly because experiments normally have been carried out with targets that are too small to be representative for semi-infinite targets. For the same reason, the evaluation of β_T and ψ_T yields a result that is too small for at least one of these parameters.

If the projectile velocity v is smaller than the characteristic velocity v_T, then the projectile may penetrate as a rigid projectile making a hole with the same diameter $D_T=d_P$ as the projectile. Otherwise it may either be stopped and partially flattened against the target surface [1] or become a ricochet, either intact or partially deformed. The ricochet cases were not considered in the previous papers.

The difficulty with the model in [3 - 5] for SC jet penetration is specification of the fragment diameter d_P. From the experimental point of view it appears more reliable to establish a relation between D_T, v, β_T, Y_T, ρ_T and the SC insert thickness t via a non-dimensional coefficient ψ_{SC}, which is different from but similar to ψ_T. The coefficient ψ_{SC} must be allowed to depend on both the SC jet and the target materials since the diameters of the SC jet fragments do not only depend on the thickness of the insert but also on the shape. Older SC:s have conical inserts whereas the shape of modern SC inserts are more like trumpets, which yield more accumulated length L_P, smaller diameter d_P and higher maximum jet velocity v_{front}. Thus the modern SC jets yield higher penetration capacity. However, at the present stage the model represented by Eqs. (1) and (2) will be used.

Model for shaped charge jet penetration

In the model for SC jet penetration in [5] it is assumed that the jet consists of molten material from the insert. For stand-off distances $S<S_{opt}$ the jet is continuous and stretching since there is a velocity gradient along the jet. For the stand-off S_{opt} the jet is assumed to become instantly fragmented. The fragments are assumed to be cylindrical with the accumulated length L_P. Initially, the distances between the fragments are negligible. In reality the fragmentation (probably) starts at the front of the jet and spreads towards the rear end, where the jet is terminated by a slowly moving slug, namely the remainder of the insert. The jet is assumed to contain the fraction α of the volume of the insert. Representative values for α with conical inserts are between 10 and 15 %. Knowledge of this fraction, of L_P and of the initial volume of the insert yields the calculated fragment diameter d_P.

Real SC jet fragments are more like prolate ellipsoids, the length of which is a few times the maximum transverse diameter, but some are so short that they are almost spherical. When the fragments are eroded against a target it is likely that the global hole shape will be determined by average parameters such as α, L_P and d_P but that it will be rather independent of the actual shape and number of fragments in the jet, at least

as long as the fragments are not significantly disturbed by previously eroded material in the manner described in [5].

In reality the fragment diameter increases slightly from the front to the rear end of the jet, but this effect is neglected here. Experimental results in [6] yield fragment diameters that are roughly 50 % greater than the thickness t of the SC insert. Knowledge of the fraction α and the assumption d_P=1.5t yield the calculated accumulated length L_P. However, the practical procedure is experimental determination of both L_P and d_P for representative SCs from radiographs, whereupon values for the corresponding ratio d_P/t and fraction α are calculated.

The fragment velocities (are assumed to) vary linearly along the jet. The velocity of the first fragment is v_{front}. Accordingly the velocity of a fragment, behind which the accumulated length of the jet is L, is v=$v_{front}L/L_P$.

For optimum (and smaller) stand-off, previously eroded jet material is (assumed to be) flying in the hole around the residual jet but with much smaller velocities than those of the jet. It is assumed that this eroded jet material does not disturb the residual jet. When a fragment with velocity v and length l_P impacts the hole bottom, the hole depth increases with the amount $\psi_T^2\,\rho_P\,l_P\,/\left(2\,\rho_T\right)$. The hole is approximately conical and ends at the depth $P_{\rm lim}$, which corresponds to the smallest fragment velocity that contributes significantly to the penetraion depth

$$v_{\rm lim}=\sqrt{\beta_T\,Y_T\left(\frac{\psi_T^2}{\rho_T}+\frac{2}{\rho_P}\right)}\,. \qquad (3)$$

This velocity corresponds to the situation when the instantaneous penetration velocity corresponds an increase rate of the hole volume around an eroding projectile that is equal to the rate of the decrease of the projectile volume. In other words, there is just enough room for the eroded projectile material without requiring a velocity of this material towards the hole entrance.

The diameter of the part of the hole that is produced by the fragment with the velocity v is (assumed to be) given by Eqs. (1) and (2). It is assumed that β_T=5 for all (relevant) target materials. When the fragment velocity v equals the limit velocity $v_{\rm lim}$, then the space between the residual projectile diameter d_P and the hole diameter D_T=$D_{T,{\rm lim}}$=$d_P v_{\rm lim}/v_T$ is only just large enough to make room for the instantaneously eroded fragment material [3]. For a copper jet and a steel target with the strength Y_T=1.0 GPa and with the penetration parameters β_T=5 and ψ_T=1.3 Eq. (3) yields $v_{\rm lim}$≈1.1 km/s. However, in reality it cannot be sufficient that the hole diameter is only just big enough, because then the eroded jet material must be deposited along the hole wall without any voids and thickness variation. Accordingly a practical value for the limit velocity $v_{\rm lim}$ is perhaps twice as big as in Eq. (3).

Subsequent fragments, with velocities v<$v_{\rm lim}$, will increase the depth of the hole slightly, but thereby they will not be completely eroded, at least not according to the suggested extension of the model in [3]. Thus, hole plugging will occur if the target thickness h is greater than

$$P_{\rm lim}\approx\frac{\psi_T^2\,\rho_P\,L_P}{2\,\rho_T}\left(1-\frac{v_{\rm lim}}{v_{front}}\right). \qquad (4)$$

The circumstance that fragments with velocities slightly smaller than $v_{\rm lim}$ will cause additional penetration, and that fragment diameters in reality increase slightly with decreasing fragment velocity v, means that $P_{\rm lim}$ from Eq. (4) can only be expected to be a rough estimate of the real hole depth P_{stop}. Experimental determination of P_{stop} normally requires that the target be cut along the axis of the hole, at least when the densities ρ_P and ρ_T are not sufficiently different so that the materials are distinguishable on radiographs. If the target is not a solid piece of material but consists of a stack of plates, then some of the plugging effect is lost since some of the eroded jet material will be extruded between the plates, even if these are close-packed. However, due to the previously emphasised uncertainties with the estimate P_{stop}≈$P_{\rm lim}$, the simpler experiments with stacked targets may nevertheless (be assumed to) be sufficiently representative for evaluation of the suggested model for SC jet penetration depth.

The estimate $P_{stop} \approx P_{\lim}$ is only applicable for optimum stand-off $S=S_{opt}$. For other stand-off for precision shaped harges (PSCs) with conical inserts an empirical relation for the penetration depth P_{stop} is suggested in [5], namely

$$P_{stop} = \frac{P_{\lim}}{1+\left(\frac{S-7C}{14C}\right)^2}, \qquad (5)$$

where C is the SC calibre. For $S<S_{opt}=7C$, Eq. (5) yields reasonable estimates of the penetration depth while the jet is stretching to reach the fragmentation length L_P. Thereby the decreasing diameter of the stretching jet with increasing stand-off must be reasonably accounted for if the corresponding conical hole diameter shall be calculated. A natural way of doing this is to increase the hole diameter that is obtained from Eqs. (1) and (2) with a certain fragment velocity v for optimum stand-off, namely $D_T=d_P v/v_T$, with the factor $\sqrt{S_{opt}/S}$.

For $S>S_{opt}$ the shape of the hole is assumed to be a truncated cone. The outer hole diameter, at the front surface of the target, is given by $D_T=d_P v_{front}/v_T$ and the inner diameter is given by $D_T=d_P v_{\lim}/v_T$. Since there is a tail of fragments with velocities $v<v_{\lim}$ that is followed by a slug, which contains between 85 and 90 % of the mass of the insert, the hole in a solid target will not be open to the depth P_{stop}. The fragments in the jet tail will plug the innermost part of the hole and the slug will be stopped at smaller depth, normally so that there is an unplugged part of the hole in front of the slug.

The reason why the penetration depth $P(S)$ decreases with increasing stand-off for $S>S_{opt}$ is (assumed to be) that when the distances between the jet fragments increase, then some of the previously eroded jet (and target) material will fly in between the fragments of the residual jet (despite the relatively low velocities of the eroded material). Consequently, the residual jet fragments will be at least partially eroded by previously eroded material before they reach the hole bottom and can contribute to the penetration depth. This effect is demonstrated via numerical simulation with Autodyn, whereby eroded material is not eliminated instantly (as is default with Autodyn, although this violates mass conservation) but remains in the calculations as flying free nodes with relevant masses [5]. Unfortunately, this simple explanation of SC jet penetration decrease with increasing stand-off seems to be very difficult to use for design of a physical model instead of the empirical relation in Eq. (5). On the other hand, the design of real SC warheads is normally such that they are used with sub-optimum stand-off $S<S_{opt}$.

Models for total mass, energy and mass distribution of target fragments from shaped charge jet perforation

When the target thickness h is smaller than the (achievable) penetration depth P_{stop}, then the SC jet will perforate the target so that the tail of the jet, and perhaps also the slug, can pass and cause damage to components behind. The velocity v_{perf} of the SC jet fragment with which the penetration depth h is reached in a semi-infinite target is obtained in analogy with Eq. (4)

$$v_{perf} \approx v_{front}\left(1-\frac{2\rho_T h}{\psi_T^2 \rho_P L_P}\right). \qquad (6)$$

The corresponding hole diameter is $D_{T,perf}=d_P v_{perf}/v_T$. In analogy with the models for rigid and eroding projectile perforation in [1 - 4] it seems reasonable to assume that perforation by a SC jet will produce a mass m_T of fragments from the rear surface of the target that, to a rough approximation, is given by

$$m_T \approx \rho_T D_{T,perf}^3. \qquad (7)$$

The exit hole is (assumed to be) roughly circular with the area $\pi D_{T,perf}^2/4$, which means that the thickness h^* of the plug with the volume $D_{T,perf}^3$ that is crushed by jet fragments to become the target fragments, is obtained from the relation

$$h^* \approx \frac{4}{\pi} D_{T,perf} \,. \tag{8}$$

If $h < h^*$ then there is no penetration phase, which means that all target material in front of the SC jet is crushed to fragments. Eq. (8) for h^* is similar to the corresponding relation for projectile perforation (in reality the plug that becomes target fragments is not cylindrical but rather a truncated cone as discussed in [4]). Accordingly, the accumulated length L_P^* of the SC jet that produces fragments from the rear target surface is (assumed to be) given by

$$L_P^* \approx \frac{2\,\rho_T\, h^{(*)}}{\psi_T^2\, \rho_P} \,, \tag{9}$$

where $h^{(*)}$ is the smaller of h and h^*. The kinetic energy of this part of the jet, the mass of which is m_P^*, is

$$W^* \approx \frac{\pi}{8} \rho_P\, d_P^2\, L_P^*\, v_{perf}^2 = \frac{1}{2} m_P^*\, v_{perf}^2 \,. \tag{10}$$

Some of this energy is required for fracturing of the plug into fragments, and the remainder is available to become kinetic energy of the fragments and the eroded jet material, in analogy with the models for rigid and eroding projectiles in [1 - 4]. Thus, a model for the fracturing energy W_{fract} should be sought. W_{fract} must depend on the way in which the plug is fractured, and generally so that it increases with the number of fragments that are produced.

A model for the distribution of fragment masses is suggested in [7] and adopted in [4]. With this model the accumulated mass $M(n)$ of the n heaviest target fragments is

$$M(n) = m_T \left\{ 1 - \exp\left(- B\, n^{\lambda} \right) \right\} \tag{11}$$

where B and λ are non-dimensional parameters to be chosen so that they describe a real distribution as accurately as possible in some appropriate sense. Values in [7] for fragments from either explosive-formed projectiles or structural casings or target plates are found in the intervals $0.07 < B < 0.26$ and $0.51 < \lambda < 0.64$, whereas two cases corresponding to projectile perforation of target plates are represented by B=0.1103, λ=0.6357 and B=0.1010, λ=0.5087. Without experimental results, from which B and λ can be determined, it is suggested in [4] that

$$B = 0.1 \tag{12}$$

and

$$\lambda = 0.5 \tag{13}$$

should be chosen to describe mass distribution of target fragments from projectile perforation. Target fragments from SC jet perforation should be treated in the same manner. Intuitively is might be expected that SC jet perforation causes a greater number of fragments in the total mass m_T than a projectile, which primarily means that the value of B should be smaller for SC jet perforation.

When $B << 1$, as in Eq. (12), the mass of the largest fragment is

$$m_1 = m_T \left\{ 1 - \exp\left(- B \right) \right\} \approx B\, m_T \,. \tag{14}$$

Similarly, the mass of the fragment with number n is

$$m_n \approx m_T\, B\, \lambda\, n^{\lambda-1} \exp\left(-B\, n^{\lambda}\right). \qquad (15)$$

If the plug, which is the origin of the target fragments, should be slowly compressed to fracture in a testing machine, then the elastic energy in the plug at the moment of fracture is given by $W_{fract} \approx Y_T^2\, D_{T,perf}^3 / \left(2\, E_T\right)$. Here E_T is the elastic modulus of the target material. When blunt-nosed rigid or eroding projectile perforation produces target fragments, the fragmentation energy is (assumed to be) [1, 4]

$$W_{fract} = \frac{\pi}{8} D_{T,perf}^2\, h^{(*)} \left(\pi\, h^{(*)} + 2\, D_{T,perf}\right) Y_T\,. \qquad (16)$$

This fragmentation energy may be regarded as the sum of a crushing energy and a cutting energy. The former is proportional to the volume $\pi\, D_{T,perf}^2\, h^*$ that is crushed and the target yield strength Y_T. The latter is proportional to the hole area $\pi\, D_{T,perf}\, h^*$ to be cut, the cutting length h^* and Y_T. The numerical factors in these two energy expressions are chosen via comparison eith experimental results.

Eqs. (7), (8) and (16) yield

$$W_{fract} \approx 3\, D_{T,perf}^3\, Y_T\,, \qquad (17)$$

which is much greater than the crushing energy in a testing machine since $E_T >> Y_T$. This is natural since the crushed plug from a testing machine contains at least a few pieces that are much bigger than the biggest fragment from projectile perforation, whereas there is very little fine-grained material. Thus the fragment distribution from a testing machine should correspond to a significantly greater value of B than in Eq. (12), whereas the value of λ is more difficult to guess.

At the present stage it does not seem to be meaningful to suggest a model for how the fracturing energy W_{fract} should depend on the distribution parameters B and λ. Consequently, some other way of estimating the kinetic energy of target fragments and eroded jet material must be sought.

Crushing and acceleration of the initially motionless target mass m_T to the final velocity v_{exit} and simultaneous retardation of the jet fragment mass m_P^* from v_{perf} to the same final velocity requires some time τ. If it is assumed that this is caused by the same action-and-reaction force F without loss of momentum to the surrounding target material, then momentum conservation yields

$$v_{exit} \approx \frac{v_{perf}}{1+\dfrac{m_T}{m_P^*}} = \frac{v_{perf}}{1+\dfrac{\psi_T^2\, D_{T,perf}^2}{2\, d_P^2}}\,. \qquad (18)$$

The fracturing energy is then obtained as the difference between the initial and final kinetic enegies

$$W_{fract} \approx W^* - \frac{1}{2}\left(m_P^* + m_T\right) v_{exit}^2 \approx \frac{W^*}{1+\dfrac{m_P^*}{m_T}}\,. \qquad (19)$$

When there is no loss of momentum, then the velocity change for the masses m_T and m_P^* must occur over the same distance. A reasonable estimate of this distance is $D_{T,perf}$. If the force F is assumed to be constant during the interaction time τ, then it is found that

$$F \approx \frac{2\, m_T\, v_{perf}^2}{\left(1+\dfrac{m_T}{m_P^*}\right)^2 D_{T,perf}} \qquad (20)$$

and

$$\tau \approx \left(1+\frac{m_T}{m_P^*}\right)\frac{D_{T,perf}}{v_{perf}}. \qquad (21)$$

However, it is very likely that in reality there will be some momentum loss caused by friction between the outer parts of the fractured plug and surrounding (not moving) target material. Thus the acceleration force on the mass m_T will be smaller than the retardation force on the mass m_P^* so that the situation must be described in a more complicated manner and involve additional parameters, for instance a coefficient of friction.

The hole diameter $D_{T,perf}$ is normally at least twice the jet diameter d_P, which means that the velocity v_{exit} in Eq. (18) is at least a couple of times smaller than v_{perf}. This conclusion seems realistic even if the conditions for the results in Eqs. (18) – (21), primarily no momentum loss to the surrounding target material and the same exit velocity for eroded jet material and target fragments, are not very well fulfilled.

The target fragments will initially be more or less united to one mass. Thus, it is understandable that jet fragments with diameters that are significantly smaller than the hole diameter $D_{T,perf}$ can contribute to acceleration of target fragments from the outer parts of the plug. Furthermore, the velocities of several subsequent jet fragments are higher than v_{exit} and these will consequently overtake the bundle of fragments from the target and eroded material from the jet. A rough estimate of the additional length of the SC jet that should contribute to the acceleration of the target fragments is

$$L_{P,add}^* \approx v_{perf}\,\tau \approx \left(1+\frac{\psi_T^2\, D_{T,perf}^2}{2\,d_P^2}\right) D_{T,perf}. \qquad (22)$$

When the diameter ratio in Eq. (22) is at least a few times greater than unity, then the contribution from later SC jet fragments to the acceleration of the target fragments should be considerable. These later fragments should primarily increase the velocity of the target fragments that are close to the SC jet. Accordingly the target fragment bundle should be expected to be similar to that in [4, Figure 2]. The same fragment bundle is also shown in Figure 1, where the eroding projectile in [4, Figure 2] is replaced by a SC jet with almost cylindrical fragments, for which $l_P \approx 2.3 d_P$. If it is assumed that the foremost-and-outmost target fragments have the velocity v_{exit} given by Eq. (18) and that the velocity variation of the foremost fragments varies with the angle ϑ in the interval $0 \le \vartheta \le \Psi$ in the same way as in [4], then the exit velocities of the foremost fragments are

$$u_{exit} = 2\, v_{exit} \cos\left(\frac{\pi\,\vartheta}{3\,\Psi}\right). \qquad (23)$$

It seems reasonable to assume that the external bundle angle Ψ should be equal to that in [4] for flat-nosed projectiles, namely $\Psi=\pi/6=30^o$.

The model in [4], which is intended to describe fragment velocities and directions of motion produced by rigid as well as eroding projectile penetration of hard metallic targets, is borrowed in several respects from [8]. However, there is a big difference in that the model in [4] accounts for all target fragments. The model in [8] only accounts for a minor fraction that is accelerated via direct contact with the residual projectile. The major fraction, which consists of considerably larger fragments than the minor fraction, is created via reflection of elastic compression waves from the rear target surface. Accordingly the velocities of the fragments from the major fraction are quite small, typically less than say 50 m/s. The velocities of the fragments in the minor fraction have significantly higher velocities, which are comparable to the exit velocity of the residual projectile.

The experimental results below in Figures 2 - 4 strongly indicate that there is a similar situation for target fragments produced by SC jet perforation, namely a large mass fraction of slowly moving fragments and a small mass fraction of significantly faster moving fragments. Even if the perforation velocity v_{perf} is significantly higher than the elastic wave velocities in the target material, the hole bottom velocity, which is

roughly given by $D_{T,perf}/\tau$, should still be considerably smaller than the wave velocities due to the mass ratio factor in Eq. (21). Consequently it is suggested that the procedure in [4] for determination of the large mass fraction of slowly moving larger fragments and the corresponding small mass fraction of rapidly moving, smaller fragments is adopted also for target fragments produced by SC jet perforation.

The diameter ratio in Figure 1 is $D_{T,perf}/d_P \approx 3$. With $\psi_T^2 = 2$ Eqs. (18) and (23) then yield $v_{perf}=10v_{exit}$ and almost twice this velocity for the fastest, innermost fragment. This fragment is at the distance about $4.5D_{T,perf}$ from the target, which means that the front fragment of the remaining SC jet should be almost at the distance $20D_{T,perf}$ from the target.

With a steel target a representative value for the characteristic velocity is v_T=1.0 km/s. With a copper jet from a SC with calibre C=84 mm representative values for the jet diameter and the front velocity are d_P=1.5 mm and v_{front}=9.3 km/s. Furthermore, the accumulated jet length to the fragment with the velocity v=3.5 km/s is L_P=85 cm. If this is the jet in Figure 1, then the perforation velocity is $v_{perf}=v_T D_{T,perf}/d_P \approx 3.0$ km/s, the fragment length is $l_P \approx 2.3 d_P \approx 7$ mm, there are initially $L_P/l_P \approx 120$ fragments with velocities greater than 3.5 km/s and the velocity difference between to successive fragments is about 50 m/s. The distance between two fragments in Figure 1 is s≈9 mm. If fragmentation is assumed to occur simultaneously along the entire length of the SC jet, then it occurred about 0.009/50 s ≈0.18 ms before the picture in Figure 1.

The accumulated length of the jet to the fragment with the velocity v_{perf}=3.0 km/s is $L_P \approx 85 \times (9.3-3.0)/(9.3-3.5) \approx 92$ cm. Accordingly Eq. (6) yields the target thickness h≈71 cm. The time required for the fragment with the velocity v_{perf}=3.0 km/s to go through target is then about 0.24 ms, which is greater than the estimated time 0.18 ms since jet fragmentation occurred. Accordingly, the jet was not stretched to the fragmentation point when the first fragment hit the target, which means that the stand-off was sub-optimal. This implies that the real target thickness is somewhat smaller than 71 cm. During the penetration stretching of the remaining jet continues until fragmentation occurs, and it should have occurred shortly before the fragment with the velocity v_{perf}=3.0 km/s reached the rear target surface.

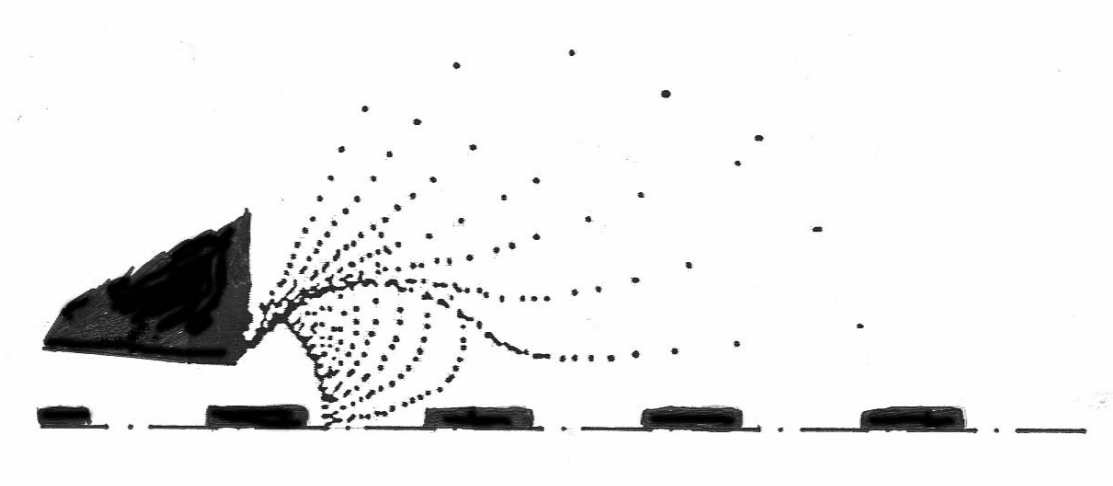

Figure 1. Production of small-and-fast target fragments in connection with SC jet perforation.

It should be emphasised that the model for target fragment velocities, represented by Eqs. (18) and (23), corresponds to an increasing number of fragments with decreasing fragment velocities u_{exit} for increasing velocity v_{perf} of the SC jet fragments that produce the target fragments. Experimental results for fragment velocities via radiographs are required to determine if this assumption is realistic. If the velocities u_{exit} should be found to increase with v_{perf}, which they actually do for eroding projectile penetration in [8], then the model must be changed so that at least some kinetic energy and momentum of the SC jet fragments corresponding to the length $L^*_{P,add}$ in Eq. (22) is transmitted to the target fragments to a greater degree.

As for the previously suggested models in [1 - 5], the intended application of the model above is in computer programs for assessment of the effects on and the vulnerability of complex targets such as tanks, fighter aircraft and naval ships. Thereby it is necessary to also specify the directions in which the target fragments travel after having left the target. However, all such additional features are assumed to be modelled reasonably well in the same way as for rigid and eroding projectiles in [4].

Comparison with experimentral results

The experimental results below are far from sufficient for validation or rejection of the relations that represenmt the model suggested above. Nevertheless, it is believed that these experimental results are representative. The scatter in such experiments is normally relatively large, as for instance for the *distributions of fragment masses* below. Unfortunatly, the verbal description of results is cumbersome to read, but a better way presenting the comparison has not come to mind.

Comparison with experimental results for the hole diameter

Experimental results in [6, Figure 2] show hole diameters in targets of steel SIS 1311, for which the density is ρ_T=7.8 g/cm^3 and the yield strength is Y_T≈0.3 GPa. The SC caliber is C=92 mm.The copper insert is conical with the bas diameter 77 mm, the half apex angle θ=21^o and the thickness t=2.3 mm. The velocity of the first SC jet fragment is v_{front}≈7.7 km/s. With about optimum stand-off, namely S=60 cm, the initial hole diameter is D_T≈40 mm. The design of a similar SC in [6, Figure 3], where the average diameter of the first 15 fragments is d_P≈2.8 mm, corresponds to the base diameter 72 mm, the half apex angle θ=25^o and the thickness t=1.9 mm. If it is assumed that the relation d_P/t≈1.5 for the latter SC is also valid for the former, then Eqs. (1) and (2) and β_T=5 yield v_T≈0.66 km/s and ψ_T≈1.5. It should be mentioned that the diameter of the very first fragment in [6, Figure 3] is significantly larger, namely d_P≈4.5 mm, and that this is neglected in the evaluation of v_T and ψ_T.

Experimental results in [9, Table 9] show hole diameters in targets of armour steel KAFT 415-8, for which the density is ρ_T=7.8 g/cm^3 and the yield strength is Y_T≈0.9 GPa. The SC caliber is C=45 mm. The copper insert is conical with the half apex angle θ=25^o and the thickness t=1.06 mm. The velocity of the first SC jet fragment is v_{front}≈7.6 km/s. With about optimum stand-off, namely S=25 cm, the initial hole diameter is D_T≈13 mm. If it is assumed againthat d_P/t≈1.5, then Eqs. (1) and (2) and β_T=5 yield v_T≈0.93 km/s and ψ_T≈1.2.

Experimental results in [10, Pages 19 and 20] show hole diameters in targets of aluminium 4212-6 and 4338-6, for which the density is ρ_T=2.7 g/cm^3 and the yield strength is Y_T≈0.25 and 0.37 GPa, respectively. The SC:s are the same as in [9]. With about optimum stand-off the initial hole diameter is D_T≈18 mm in both targets. In these cases Eqs. (1) and (22), d_P/t≈1.5 and β_T=5 yield v_T≈0.67 km/s and ψ_T≈1.0 and 0.8, respectively.

Comparison with experimental results for the distribution of fragment masses

Experimental results for the mass m_T and the distribution $M(n)$ are obtained from SC:s with caliber C=45 and 84 mm and reported in [11]. Comparison with [5, Figure 1] and experimental results for the relation between penetration depth and stand-off for these SC:s show that the greater should be P(recision)SC:s and the smaller are quite close to PSC:s. Furthermore the relation between accumulated jet length and fragment velocity is practically linear as assumed in the model.

The smaller SC:s were tested at stand-off S=80 mm or S≈1.8C and the larger at S=175 mm or S≈2.1C. These stand-off distances are respresentative for built-in stand-off for real warheads of similar caliber.

In the experiments, the SC jet perforates the target plate in the vertical downwards direction. The residual SC jet is stopped by an aluminium target at the bottom of a water tank with the diameter 1.0 m. The fragments are stopped by the water and collected from the bottom of a stainless strainer, with slightly smaller external dimensions than the inside of the tank and only allowing passage of particles with smaller diameter than about 0.10 mm, after lifting the strainer out of the tank. The steel fragments from the target are separated magnetically from copper fragments from the jet and aluminium fragments from the stopping target. The steel fragments are weighed together to determine the total mass m_T and individually, with a high precision scale and starting with the larger fragments, to determine the distribution $M(n)$. It should be emphasised that all fragments from the rear target surface are collected with this method, in contrast to the experiments behind the results in [8] where only the minor fraction with small-and-fast fragments was recovered and evaluated. The total fragment mass in [8] was determined via the mass reduction of the target, which includes fragments ejected from the impacted surface. For this reason the targets in [8] were small, with an initial external diameter that was onlyabout twice the diameter of the hole.

The mass m_1 of the heaviest fragment in a distribution is between 0.1 and 1.0 g for the smaller SC:s and about 6 g for the greater SC. The mass of the smallest fragment that is determined for a particular distribution ranges from 0.001 to 0.007 g. The number of fragment masses that iere measured ranges from about 40 to 300. The ratio between the sum of the determined fragment masses and the total mass ranges from about 40 to 90 %.

From [11, Figures 16 and 17] it is seen that the (evaluated) accumulated length and total mass of jet fragments from the smaller SC for fragment velocities in the interval $3.0<v<v_{front}\approx 7.6$ km/s are $L_P\approx 0.30$ m and $m_P\approx 2.5$ g, respectively. The apex angle of the copper insert is $2\theta=50^o$, the mass is 27 g and the thickness is $t=1.06$ mm. If the jet is assumed to consist of cylindrical fragments (instead of approximately prolate ellipsoids), then the corresponding fragment diameter is $d_P\approx 1.1$ mm. Thus, the ratio d_P/t from [11] is somewhat smaller than that from [6].

Five tests with the smaller SC against a steel armour plate with thickness $h=25$ mm and hardness HB360, corresponding to $Y_T\approx 1.2$ GPa, are reported. The recovered mass of target fragments ranges from 8.6 to 15.2 g with the average $m_T=11.6$ g. With the target velocity parameter $\psi_T\approx 1.3$ from [3] and $\beta_T=5$ the characteristic target velocity is $v_T=\psi_T\sqrt{\beta_T\, Y_T/\rho_T}\approx 1.1$ km/s. Since the stand-off $S=80$ mm is slightly less than $S_{opt}/2\approx 10$ cm the hole diameter close to the front surface should be expected to be slightly more than $D_T\approx d_P v_{front}/v_T\approx 7$ mm multiplied by $\sqrt{2}$, which yields about 10 mm. The measured value at about the depth 10 mm is $D_T\approx 11$ mm. It should be mentioned that there is only negligible global bending of the target plate around the hole.

The target thickness $h=25$ mm is so small compared to $P_{stop}\approx 0.23$ m that the hole can be assumed to be roughly cylindrical (although there are conical craters at both ends). Accordingly, the assumption in Eq. (7) yields the total mass $m_T\approx\rho_T\, D_T^3\approx 10.4$ g, which is in reasonable agreement with the average value 11.6 g above. It should be emphasised that the corresponding volume is about one third of the total hole volume. Some target fragments are ejected backwards from the front suface, but at least about half of the whole hole volume is doubtlessly produced without target erosion and hence via elastic-plastic deformation (expansion) of the material around the hole.

The mass of the heaviest fragment ranges from 0.3 to 0.7 g (the real values are with three decimals) with the average $m_1\approx 0.5$ g. The mass of the 20 heaviest fragments ranges from 2.8 to 4.5 g with the average $M(20)\approx 3.7$ g. With the average total mass $m_T\approx 11.6$ g and the average mass for the heaviest fragment Eq. (14) yields $B\approx 0.043$, whereupon Eq. (11) and $n=20$ yield $\lambda\approx 0.78$. The choise of the number $n=20$ here and below is rather arbitrary. Other numbers such as $n=5$ or 10 or 40 will yield different but similar values for λ. It is believed that the heaviest target fragments are most important in the intended applications of the model. Consequently the number n should not be very much larger than unity.

In order to quantify the scatter it is reasonable to evaluate the parameters B and λ for each of the five tests in the same manner as for the average values above. Thus, the five results $B\approx 0.027$ & $\lambda\approx 0.82$, $B\approx 0.033$ & $\lambda\approx 0.72$, $B\approx 0.048$ & $\lambda\approx 0.74$, $B\approx 0.067$ & $\lambda\approx 0.72$ and $B\approx 0.070$ & $\lambda\approx 0.56$ are obtained.

Three tests with the smaller SC against a package of four steel armour plates of the same quality but with thickness 10 mm, corresponding to $h=40$ mm, are reported. The recovered mass of target fragments ranges from 7.6 to 9.3 g with the average $m_T=8.3$ g. The photograph from these tests only shows the hole in (one of) the fourth plate(s). The front side diameter of this hole is $D_T\approx 10$ mm. Thus $m_T\approx\rho_T\, D_T^3\approx 7.8$ g is also in reasonable agreement with the experimetal result. In this case there is significant global bending of the plate around the hole. The front surface is displaced about 5 mm along the edge of the hole and the bending displacement disappears at about the diameter 3 cm. Although it is not shown or mentioned in [6] it is known that there is similar but less global deformation of the third plate and only little of the second plate.

The mass of the heaviest fragment ranges from 0.7 to 1.0 g with the average $m_1\approx 0.9$ g. The mass of the 20 heaviest fragments ranges from 4.0 to 6.5 g with the average $M(20)\approx 4.9$ g. With the average total mass and the average mass for the heaviest fragment Eq. (14) yields $B\approx 0.11$, whereupon Eq. (11) and $n=20$ yield $\lambda\approx 0.70$.

Three tests with the smaller SC against a package of ten steel armour plates, corresponding to $h=100$ mm, are also reported. The recovered mass of target fragments ranges from 1.9 to 3.5 g with the average $m_T=2.7$ g. The photograph from these tests shows the hole in (one of) the tenth plate(s), the front diameter of which is $D_T\approx 7$ mm. Thus $m_T\approx\rho_T\, D_T^3\approx 2.7$ g is once again in reasonable agreement with the experimental result. In this case there is considerably smaller global bending of the plate than for the previous case. The front surface is displaced about 2 mm along the edge of the hole and the bending displacement disappears at about the diameter 2 cm.

The mass of the heaviest fragment ranges from 0.1 to 0.2 g with the average $m_1\approx 0.13$ g. The mass of the 20 heaviest fragments ranges from 0.7 to 1.1 g with the average $M(20)\approx 0.93$ g. With the average total mass

and the average mass for the heaviest fragment Eq. (14) yields $B\approx0.048$, whereupon Eq. (11) and $n=20$ yield $\lambda\approx0.72$.

All tests mentiond above are for normal impact. There are also results from three tests when the SC jet is at the angle $\pi/3=60^o$ to the normal. The target, which consists of two of the 10 mm thick steel plates, then corresponds to a "line-of-sight" thickness $h=40$ mm, which equals the thickness in the second set of tests above. The recovered mass of target fragments ranges from 3.4 to 6.9 g with the average $m_T=4.7$ g. This is significantly smaller, roughly with the factor $\cos(\pi/3)$, than for normal impact with the same "line-of-sight" thickness. Since oblique impact is not considered in the present paper this result is only mentioned to emphasise that the model must be extended to cover such situations before it can be put to use in the intended applications. Such extension must probably be rather empirical, for instance so that the mass m_T for normal exit after perforation along the line-of-sight thickness is reduced with the cosine of the angle between the jet and the normal direction for the rear surface of the target, as for the case in [6].

Only one test is reported with the greater SC since this test damaged the equipment so that it could not be used without major repair. The target is two steel armour plates with thickness 40 mm and hardness HB300, which corresponds to $Y_T\approx1.0$ GPa. The recovered mass of target fragments is $m_T=136$ g. There is only marginal global bending of the second plate around the hole, the diameter of which is $D_T\approx23$ mm. The target thickness $h=80$ mm is so small compared to $P_{stop}\approx0.6$ m that the hole can be assumed to be cylindrical (there is a roughly semi-spherical exit crater, the diameter of which is about 45 mm). Accordingly the assumption in Eq. (7) corresponds to the total mass $m_T\approx\rho_T D_T^3\approx95$ g, which is significantly smaller than the experimental value above but of right magnitude. However, the relative scatter around the average for the first five tests with the smaller SC above is about ± 30 %. Thus, it is quite possible that more tests with the larger SC would yield an average value in reasonable agreement with Eq. (7).

With the target velocity parameter $\psi_T\approx1.3$ from [3] and $\beta_T=5$, the characteristic target velocity is $v_T=\psi_T\sqrt{\beta_T Y_T/\rho_T}\approx1.0$ km/s. From [6, Figures 19 and 20] it is seen that the (evaluated) accumulated length and mass of jet fragments from two SC:s for fragment velocities in the interval $3.5<v\le v_{front}=9.3$ km/s are $L_P\approx0.85$ and 0.85 m and $m_P\approx12$ and 15 g, respectively. If the jet consists of cylindrical fragments, then the corresponding fragment diameters are $d_P\approx1.4$ and 1.6 mm, respectively. With the larger value the model $D_T\approx d_P v_{front}/v_T$ for the initial hole diameter at (and beyond) optimum stand-off yields $D_T\approx14$ mm. Since the stand-off $S=175$ mm is about 30 % of optimum stand-off $S_{opt}\approx0.6$ dm the hole diameter should be expected to be about $14/\sqrt{0.30}\approx26$ mm, which is in reasonable agreement with the experimental value 23 mm.

The mass of the heaviest fragment is $m_1\approx6$ g, and the mass of the 20 heaviest fragments is $M(20)\approx62$ g. Thus Eqs. (14) and (11) yield $B\approx0.044$ and $\lambda\approx0.87$. These values are of the same magnitude as those obtained from the smaller SCs, whereas the mass m_1 is larger with a factor given by the calibre ratio to the third power (as it should be expected to be).

Comparison with experimental results for the velocities of target fragments

In order to determine velocities of target fragments radiographs have been taken, two of which are shown in Figure 2. The time delay between these is $\tau_d=70$ μs. The SC calibre is $C=45$ mm, the stand-off is S=30 cm and the target thickness is h=20 mm. The optimum stand-off is $S_{opt}\approx0.20$ m and the corresponding penetration depth is $P_{\lim}\approx0.22$ m. Eq. (5) yields the penetration capacity $P(S)\approx P_{\lim}/\{1+(S/S_{\rm opt}-1)^2/4\}\approx0.20$ m. The front velocity is $v_{front}\approx7.6$ km/s and the perforation velocity $v_{perf}\approx7$ km/s is slightly smaller. The scale in Figure 2 is the same as in Figure 3, from which the estimated diameter of the SC jet fragments is $d_P\approx1.5$ mm. However, the uncertainty in this value is rather large.

In connection with perforation, a "ring" of material is broken off around the exit hole in Figure 2. The front of the ring has moved about 10 mm during the delay time, so that the velocity is about 150 m/s. This picture corroborates the assumption that target fragments from SC jet perforation should be considered to consist of two groups, namely a major fraction with large and relatively slowly moving fragments and a minor fraction with small and relatively fast moving fragments.

The first photo, to the right in Figure 2, shows that the minor fraction contains two rather diffuse and flat layers of target fragment at distances $s_1\approx36$ and $s_1'\approx57$ mm from the rear target surface. These layers are at distances about $s_2\approx90$ and $s_2'\approx150$ mm in the second photo, to the left in Figure 2. The right half of the first photo and the left half of the second photo overlap and disturb each other, but the other (outer) halves are undisturbed.

The flat layers correspond to diverging rings of fragments moving in directions that correspond to the angle $\Psi \approx 35^o$. The fragment velocities are $u=(s_2-s_1)/\{\tau_d \cos(\Psi)\}$, which yields $u \approx 0.9$ and 1.6 km/s, respectively. The rings should have started almost simultaneously from the rear target surface, namely $\tau_b = s_1 \tau_d / (s_2 - s_1) \approx 47$ μs and $\tau_b' = s_1' \tau_d / (s_2' - s_1') \approx 43$ μs before taking the first photo. Accordingly a SC jet fragment with the velocity $v_{perf} \approx 7$ km/s should be at the distance $v_{perf} \tau_b \approx 0.30$ m from the rear target surface in the first photo.

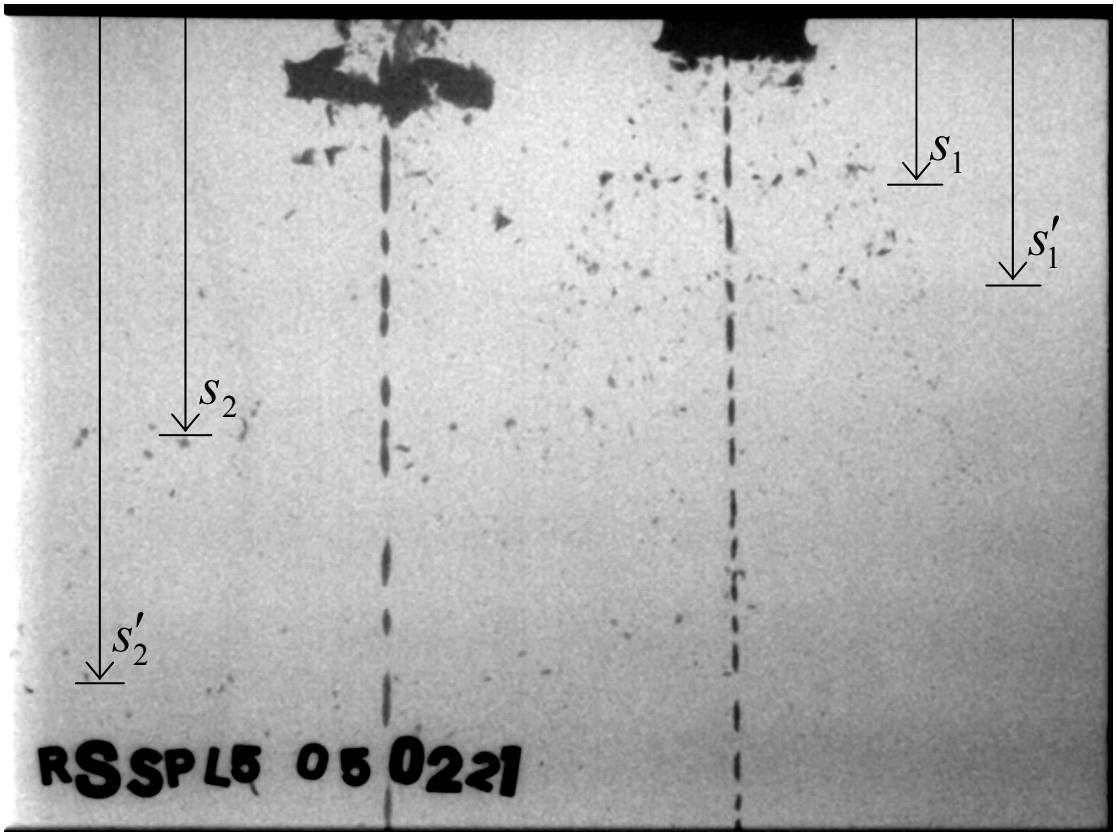

Figure 2. Original radiograph of SC jet and target fragments with 70 μs delay between the first photo (to the right) and the second (to the left). Same scale as in Figure 3 below.

It is possible to distinguish smaller target fragments that are moving up to $u_{max} \approx 2.8$ km/s, in the undisturbed (right) side of the first photo in Figure 2. All observable target fragments in this half are manually blackened in Figure 3. The contours of the fragments with velocities up to $u \approx 1.7$ km/s in the other (left) half are also blackend in Figure 3 in both the first and the second photo. The picture of the faster fragments in the left haft of the first photo is mixed with slower fragments in the second photo so they cannot be identified.

The picture in Figure 1 is the result of an axi-symmetric calculation. If all the front fragments are of the same size, then each front point represents a fragment ring, in which the number of fragments is proportional to $\sin(\vartheta)$ where ϑ is the angle between the direction of motion and the SC jet direction. In Figure 1 these angles are $\vartheta \approx j\Psi/7$ with j=1, 2, …7 and $\Psi \approx 60^o$. Thus, the outermost front point corresponds to about $\sin(60^o)/\sin(60^o/7) \approx 6$ times as many fragments as the innermost front point.

Figures 2 and 3 show the projection on a plane of the real three-dimensional bundle of target fragments. If the "occurrence" of each point in Figure 1 is imagined to be "normalized" with the weight factor $\sin(\vartheta)$ and "compressed" from $\Psi \approx 60^o$ to $\Psi \approx 35^o$, then this "normalised and expanded" picture will be fairly equal to blackened fragment bundle in Figure 3.

The experimentally observed maximum target fragment velocity $u_{max} \approx 2.8$ km/s is about 40% of the calculated maximum residual jet fragment velocity $v_{perf} \approx 7$ km/s. It is physically obvious that u_{max} must be smaller than v_{perf}, but presently a convincing physical model for the ratio between these two velocities remains to be suggested. Accordingly it is proposed that the empirical relation

$$u_{\max} = 0.4 v_{perf} \qquad (24)$$

should be used until a better empirical or theoretical model is put forward.

Figure 4 shows two photos from an identical experiment as that in Figure 3. The general features of the picture of the target fragments in the right half of the first photo in Figure 4 are quite similar to those in Figure 3.

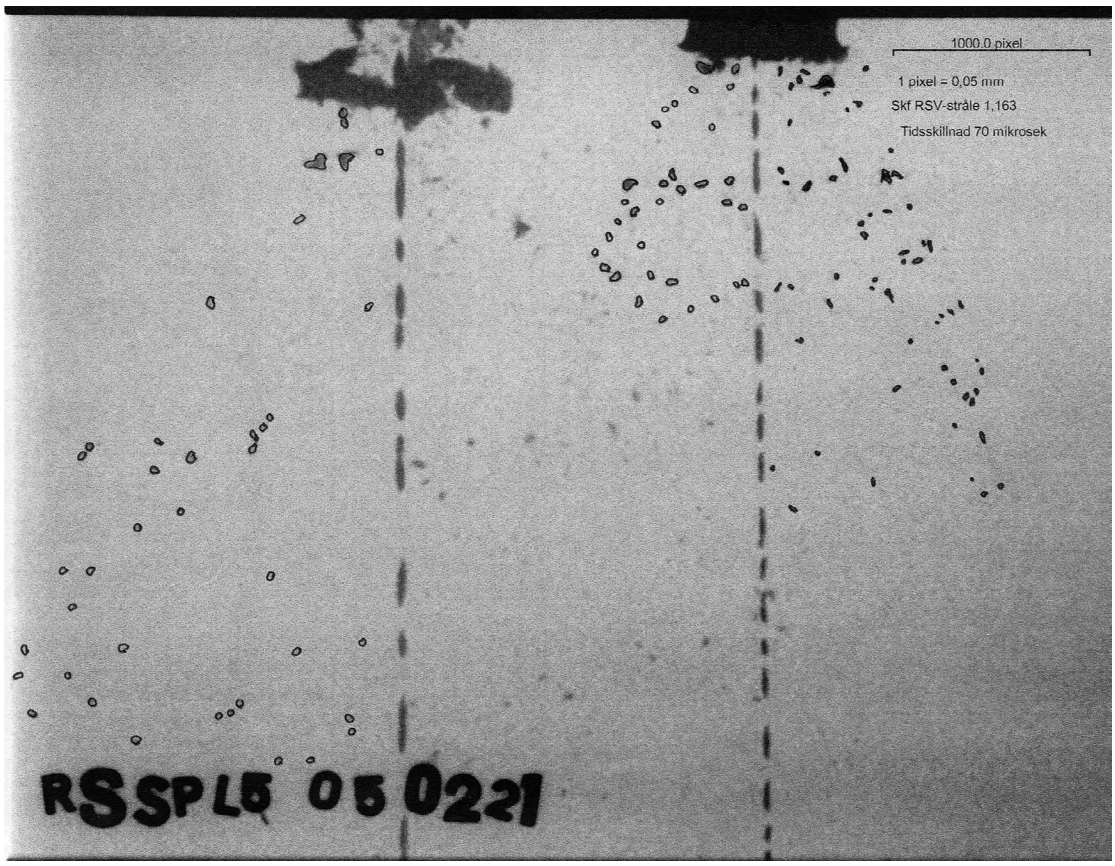

Figure 3. Same case as in Figure 2. Fragments in regions that are not covered by both photos are manually blackened for better visability. The length in the upper right corner is 50/1.163≈43 mm.

Discussion and conclusions

The general conclusion is that the models for the total mass and the corresponding distribution for target fragments from SC jet perforation yield realistic results. Stochastic variation of relevant quantities, especially the non-dimensional distribution parameters B and λ, is considerable, as it should be expected to be. In the intended applications for the model, namely in large computer programs for assessment of the effects on and the vulnerability of complex targets such as tanks, fighter aircraft and naval ships, such variation is easily accounted for when the program is based on Monte Carlo for determination of the outcome of situations with probability spectra.

The physical models in previous and the present paper make it possible to use experimental results in small scale to predict results in full scale with reasonable accuracy. Accordingly necessary experimental work can be restricted with respect to costs and resources.

The experimental values for the fragment distribution parameters B and λ for SC jet perforation differ from those for projectile perforation in the expected manner. More specifically, the value for B is about twice as big for projectiles, whereas the value for λ is closer to unity for SC jets. These differences correspond to relatively smaller target fragments from SC jets than from projectiles.

It is interesting to consider the variation of the two distribution parameters obtained from the tests with the smaller SCs for three different target thicknesses, namely h=25 mm, $h = 4\times10 = 40$ mm and $h = 10\times10= 100$ mm, which yield $B\approx0.043$ and $\lambda\approx0.78$, $B\approx0.11$ and $\lambda\approx0.70$ and $B\approx0.048$ and $\lambda\approx0.72$, respectively. The target fragments are produced with jet fragments of practically equal size, but the jet

fragment velocities decrease with increasing target thickness. The variation of the parameter B is rather disturbing, at least at first sight. It would be much more satisfactory if the value for B from $h=4\times10=40$ mm had been about equal to the other two values, because then the results could perhaps be generalised to an "universal" model. For instance, the values $B\approx0.044$ and $\lambda\approx0.87$ for (the only test with) the larger SC are quite close to the first and third pair of values for the smaller SCs.

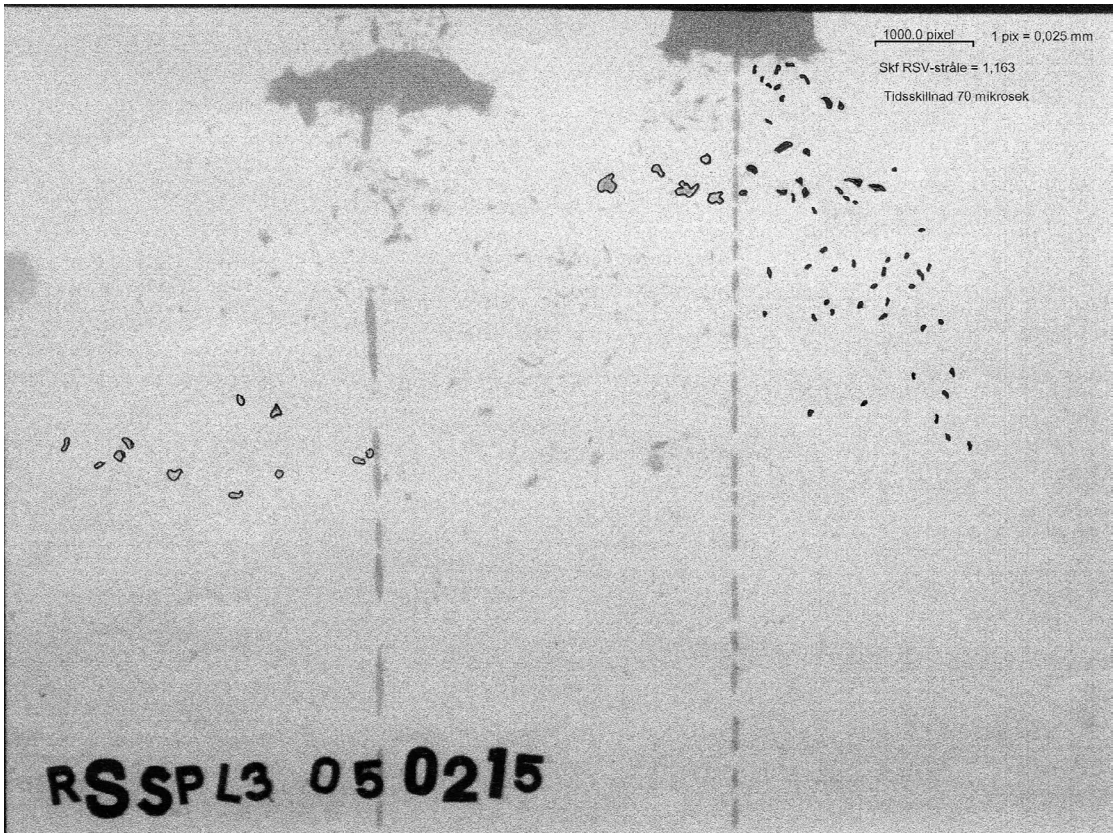

Figure 4. Identical case to that in Figures 2 an 3. Certain fragments in regions that are not covered by both photos are manually blackened for better visability. The length in the upper right corner is 21.5 mm.

Is there perhaps a natural reason for the behaviour of B above? For the deviating case with $B\approx0.11$, the exit hole diameter $D_T\approx10$ mm is practically equal to the thickness of the last plate in the target, namely $h/4=10$ mm. This manifests itself in terms of significant global bending of the last plate, contrary to the two other cases, for which the plate or last plate thickness is significantly greater than the exit hole diameter and global bending is (almost) negligible. If there is great global bending in connection with perforation, then it is likely that a few large tension cracks in the rear surface of the (last) target plate will occur as the initial stage of target fragment production, and that such cracks will join to produce fragments that are bigger than for perforation without global bending.

When SC jet penetration is studied, then it is practical and probably sufficiently realistic to use targets that consist of stacked plates to represent solid targets. Some eroded jet material will be extruded between the plates so that hole clogging is delayed, but this effect should be of minor importance for P_{stop}. However, when SC jet perforation is studied, then the thickness of the last plate in a stacked target should be significantly greater than the (anticipated) exit hole diameter if the details of the perforation phase, in particular the production of fragments, should be representative for solid targets.

The stand-off distances used in [6] are rather small compared to optimum stand-off, but they are quite representative for the normally built-in stand-off of real warheads. Accordingly it should not be first priority to study production of target fragments for optimum or beyond optimum stand-off. However, it is presently the belief of the author that such situations are quite similar to that of sub-optimum stand-off, at least for moderately great stand-off, say less than three or four times optimum stand-off.

References

1. G. Wijk, M. Hartmann and A. Tyrberg: A model for rigid projectile penetration and perforation of hard steel and metallic targets. Swedish Defence Research Agency, FOI-R--1617--SE, April 2005.
2. G. Wijk, Initially increasing penetraion resistance, friction and target size effects in connection with rigid projectile penetration and perforation of steel and metallic targets. Swedish Defence Research Agency, FOI-R--1631--SE, April 2005.
3. G. Wijk, M. Hartmann and A. Tyrberg: A model for eroding projectile penetration of metallic targets. Submitted for publication in *International Journal of Impact Engineering*.
4. G. Wijk, A model for fragmentation of hard metallic targets due to projectile perforation. FOI-R--1733--SE, October 2005
5. G. Wijk and A. Tjernberg, Shaped charge jet penetration reduction with increasing stand-off. FOI-R--1750--SE, October 2005
6. G. Wijk, A new mathematical model for the relation between stand-off and penetration for shaped charge jets. FOI-R--0361--SE, January 2002.
7. M. Held, Fragment mass distribution of "secondary fragments". *Propellants, Explosives, Pyrotechniques*, Vol. 16, pp. 21-26, 1991.
8. A. L. Yarin, L. V. Roisman, K. Weber & V. Hohler. Model for ballistic fragmentation and behind-armor debris. *International Journal of Impact Engineering*, Vol. 24, pp. 171-201, 2000.
9. J. Ekberg, RSV mot stålpansar. FOA Rapport C 20405-04, April 1981.
10. J. Ekberg, RSV mot aluminium. FOA Rapport C 20348-04, Mars 1980.
11. Å. Collin & U. Petterson, Uppfångning av sekundärsplitter vid pansarperforation med riktad sprängverkan. FOI-RH--0109--SE, Maj 2002.